Biosensors and Bioelectronics 134 (2019) 16–23

Contents lists available at ScienceDirect

Biosensors and Bioelectronics

journal homepage: www.elsevier.com/locate/bios

Graphene-based fully integrated portable nanosensing system for on-line detection of cytokine biomarkers in saliva

Zhuang Hao[a], Yunlu Pan[a,*], Wenwen Shao[a], Qiao Lin[b], Xuezeng Zhao[a,**]

[a] Key Laboratory of Micro-systems and Micro-structures Manufacturing, Ministry of Education and School of Mechatronics Engineering, Harbin Institute of Technology, Harbin, Heilongjiang, 150010, China

[b] Department of Mechanical Engineering, Columbia University, New York, NY, 10027, USA

ARTICLE INFO

Keywords:
Graphene
Saliva
Portable system
Wireless sensing
Aptamer

ABSTRACT

Saliva has been reported to contain various cytokine biomarkers which are associated with some severe diseases such as cancers. Non-invasive saliva diagnosis using wearable or portable devices may pave a new avenue for monitoring conditions of the high risk population. Here, a graphene-based fully integrated portable nanosensing system, the entire size of which is smaller than a smart-phone and can be handheld, is presented for on-line detection of cytokine biomarkers in saliva. This miniaturized system employs an aptameric graphene-based field effect transistor (GFET) using a buried-gate geometry with HfO_2 as the dielectric layer and on-line signal processing circuits to realize the transduction and processing of signals which reflect cytokine concentrations. The signal can be wirelessly transmitted to a smart-phone or cloud sever through the Wi-Fi connection for visualizing the trend of the cytokine concentration change. Interleukin-6 (IL-6) is used as a representative to examine the sensing capability of the system. Experimental results demonstrate that the nanosensing system responds to the change of IL-6 concentration within 400s in saliva with a detection limit down to 12 pM. Therefore, this portable system offers the practicality to be potentially used for non-invasive saliva diagnosis of diseases at early stage.

1. Introduction

Human saliva is an attractive clinical diagnostic bio-medium containing various cytokine biomarkers, of which the abnormal elevation levels in blood and related bodily fluids including saliva, tears and sweat (Afsahi et al., 2018; Emaminejad et al., 2017; Gao et al., 2016; Park et al., 2018), have been reported in subjects with many severe diseases such as prostate, breast and pancreatic cancer (Blay et al., 1992). Compared with tears and sweat, saliva has reasonable correlations with blood levels of numerous biomarkers and can be easily collected without any external stimulus, thus dramatically avoiding the risk of infection and the discomfort resulted from the tests with skin-piercing for blood sampling and providing a convenient alternative for non-invasive diseases diagnosis at their early stage. Hence, developing instant and convenient saliva diagnosis using wearable or portable sensing devices which are amenable to monitor conditions of the high risk population is of great significance.

Efforts have been taken out to develop technologies for non-invasive detection of cytokines and other related biomarkers in saliva (Arakawa et al., 2016; Campos et al., 2018; Chekin et al., 2018; Kim et al., 2014; Santana-Jiménez et al., 2018). Commercial methods such as enzyme-linked immuno-sorbent assay (ELISA) and bead-based immunoassay processes, can achieve highly specific and sensitive detection of cytokines, but require labor-intensive sample labeling and longtime off-line assay processes (Bariya et al., 2018; Yang and Gao, 2018). Then label-free, highly sensitive and specific detecting technologies such as electrochemical impedance spectroscopy (EIS) measurement (Bellagambi et al., 2017), chronoamperometric (CA) analyses(Barhoumi et al., 2018) and differential pulse voltammograms (DPV)(Chekin et al., 2018) are widely employed in the traditional electrochemical immunosensors for the determination of cytokine levels using target cytokine receptors (e.g., aptamers, antibodies and enzymes) at the expense of complicated operation with sophisticated bulky instruments. Moreover, the time-consuming off-line assay is still inevitable. Very recently, wearable or portable sensors such as silk dental tattoo device (Mannoor et al., 2012), radio-frequency identification (RFID) tri-layers sensor (Tseng et al., 2018), mouthguard amperometric sensor(Kim et al., 2015) and cavitas sensor (Arakawa et al., 2016), are demonstrated for simple sensing salivary biomarkers such as uric acid (Kim et al., 2015), glucose (Arakawa et al., 2016; Santana-Jiménez et al., 2018), metabolites (Kim

* Corresponding author.
** Corresponding author.
E-mail address: yunlupan@hit.edu.cn (Y. Pan).

https://doi.org/10.1016/j.bios.2019.03.053
Received 23 January 2019; Received in revised form 13 March 2019; Accepted 26 March 2019
Available online 29 March 2019

et al., 2014; Liao et al., 2015), lactate(Kim et al., 2014) and bacteria (Mannoor et al., 2012). These sensors can not only realize label-free and direct biomarkers detection but also respond to the concentration change in a few minutes or even real-time without further tedious off-line analysis. Unfortunately, due to the unwanted background interference in human saliva, such wearable (Liao et al., 2015; Tseng et al., 2018) or portable (Pruna et al., 2018) sensors with limited sensitivity and specificity are not likely to be capable of detecting complex salivary cytokine biomarkers such as the pancreatic cancer biomarker interleukin-6 (IL-6), the normal physiological level of which is around 4 pM (nearly 1000 times lower than other biomarkers) (Blay et al., 1992; Fan et al., 2014; Gasche et al., 2011). Whereas individuals with various disease states have elevated IL-6 physiological levels up to 200 pM (Khosravi et al., 2017).

Graphene, attracting a substantial amount of attention because of its excellent electrical properties (e.g. mobility of $\sim 10^4\,cm^2\,V^{-1}\,s^{-1}$ at $\sim 25\,^{\circ}C$), is extremely sensitive to its surface charge distribution, which can be transduced into a detectable change within tens of milliseconds with the aid of a field effect transistor configuration, thus enabling real-time monitoring (Hao et al., 2017; Kim et al., 2017; Park et al., 2018). Compared to conventional receptors such as antibodies which degrade significantly with increasing storage time (> 24 h) at 4 °C (Hao et al., 2018), aptamers, owing distinctive advantages such as smaller size, higher stability, long shelf life, batch-to-batch uniformity and synthetic availability (Wang et al., 2018), are more suitable to be applied in sensors towards long-term portable applications (Bariya et al., 2018). As a result, aptameric graphene-based field effect transistor (GFET) seems to be a promising alternative for specifically and sensitively detecting complex molecules such as salivary cytokines, since it has already been demonstrated in successful detection of DNA (Cai et al., 2014; Ping et al., 2016), ions (Li et al., 2017) and cells (Yang et al., 2017). However, incorporating the aptameric GFET in a portable or wearable biosensing devices still remains challenging since: (1) Existing GFETs are generally constructed as a solution-gated configuration typically requiring an external Ag/AgCl electrode, which hinders the integration and miniaturization of the device. The electrode is inserted into the solution that is in contact with graphene to supply the gating electrical field, while the electric double layer (EDL) formed at the solution-graphene interface plays the role of the gate dielectric. The capacitance across the EDL dielectric layer is susceptible to disturbances in the testing solution, which can result in fluctuations in electrical measurements of properties of graphene (Wang et al., 2016; Zhu et al., 2015). Additionally, the gating electrical field penetrating the sample solution may also disturb the affinity binding between the charged cytokines and receptors, thereby affecting the sensing stability through the electrostatic force (Van Der Heyden et al., 2005). (2) Solid-gated GFETs using SiO_2 as dielectric layer with the underlying silicon serving as the gate electrode can eliminate the need for the cumbrous electrode. However, because of the low permittivity of SiO_2 ($\varepsilon = 3.9$), 40–50V operating gate voltage V_g, which is insecure for human, is required (Chen et al., 2008). (3) Currently, measurements using GFETs have to be conducted with sophisticated sourcemeter in order to supply a tiny but steady drain-source voltage down to a few millivolts since even hundreds millivolts would burn-out the graphene channel. To date, this is still one of the challenges and impedes their wearable or portable applications.

In this paper, a graphene-based fully integrated portable nanosensing system, the entire size of which is smaller than a smart-phone and can be held in one hand (Fig. 1a), for convenient on-line detection of cytokine biomarkers in saliva with high sensitivity and specificity is presented. Further, cytokine IL-6 is used to examine the sensing capability of this nanosensing system as a representative. The miniaturized nanosensing system employs an aptameric GFET nanosensor and on-line signal processing circuits, which are integrated on printed circuit boards (PCBs), to realize signal transduction, processing, display and wireless transmission. With a novel buried-gate geometry, our GFET employs a planar golden electrode, which is defined on the substrate and buried by a 30 nm HfO_2 dielectric layer, serving as the gate, thus eliminating the need for the external gate electrode. Further, thanks to the high permittivity of HfO_2 ($\varepsilon = 16$), insecurely high operating gate voltages is also needless. With the aid of customized on-site signal processing circuits, this handheld device can provide accurate detection information of cytokine levels in saliva on an embedded liquid crystal display (LCD) screen. Also, it can transmit the information wirelessly to a smart-phone through an on-board Wi-Fi module for on-line visualizing the trend of the cytokine concentration change. Additionally, these information can be uploaded to the cloud sever through Wi-Fi connection so that health conditions of patients can be remotely monitored by doctors (Fig. 1b and c).

Detection of IL-6 is allowed by the structural change of the graphene surface immobilized specific aptamer when interacting with IL-6. Since graphene is immersed in the solution, an electrical double layer (EDL) is formed on the graphene-liquid interface. Cytokine IL-6, whose isoelectric point (PI) is ranging from 4.0 to 5.3, is weakly and negatively charged at pH 7.4. As shown in Scheme S1, absence of IL-6, the graphene surface immobilized aptamer is in an unfolded, loop and flexible state. Upon affinity binding with IL-6, it folds into a compact and stable formation. These structural changes bring the negatively charged IL-6 to the close proximity of the graphene surface, possibly resulting in the direct binding of aromatic amino acids in IL-6 with graphene through $\pi-\pi$ stacking interactions and subsequently altering the charge distribution on the graphene-liquid interface. As a result, equivalent positive charges are electrostatically induced on the other side of the interface, thereby generating equivalent free electron carriers in the bulk of graphene and yielding detectable changes in the carrier concentration as well as the measured drain-source current I_{ds} (Fig. 1d) (Hao et al., 2017; Li et al., 2017; Wang et al., 2016). It is noted that higher graphene transconductance ($g_m = \partial I_{ds}/\partial V_g$), the value of which is a suggested measure of the sensitivity of graphene, enables a greater conductivity change reflecting a unit charge excitation and can be modulated by applying external gate voltage (Wang et al., 2016). Hence, with applying a gate voltage at a calculated value, the level of g_m, as well as the response capability of I_{ds} to the external stimulus such as electron transfer, can reach its maximum, thereby enabling detection of IL-6 at an optimal sensitivity. Further explanation is detailed in the Supporting Information (Fig. S1).

Experimental results demonstrate that the developed portable device responds to IL-6 concentration changes within 400s in human saliva samples with a detection limit down to 12 pM, which is within the physiological level of IL-6. Therefore, this fully integrated portable nanosensing system offers the practicality to be potentially used for daily salivary cytokine biomarkers detection for early stage diseases diagnosis.

2. Experimental and methods

2.1. Chemicals and materials

Chemical vapor deposition (CVD) graphene was purchased from Graphenea (Cambridge, MA). 285 nm SiO_2/Si was ordered from UniversityWafer (Boston, MA). Human IL-6, human Growth Hormone (GH) and human Epidermal Growth Factor (EGF) were purchased from ACRO Biosystems (Newark, DE). Phosphate buffered saline (PBS) was purchased from Thermo Fisher Scentific (Waltham, MA). 1-Pyrenebutanoic acid succinimidyl ester (PASE) and dimethylformamide (DMF) were purchased from Sigma-Aldrich (St. Louis, MO). IL-6-specific aptamer (sequence 5′-NH_2- GGT GGC AGG AGG ACT ATT TAT TTG CTT TTC T -3′) was synthesized and purified by Sangong Biotech (Shanghai, China). The commercial disaccharide dry ease run gargle sample was purchased from Success Bio-Tech (Shandong, China). The sterile synthetic swab for human saliva sampling was ordered from Salivette (Sarstedt, Germany). The controller chips employed the signal

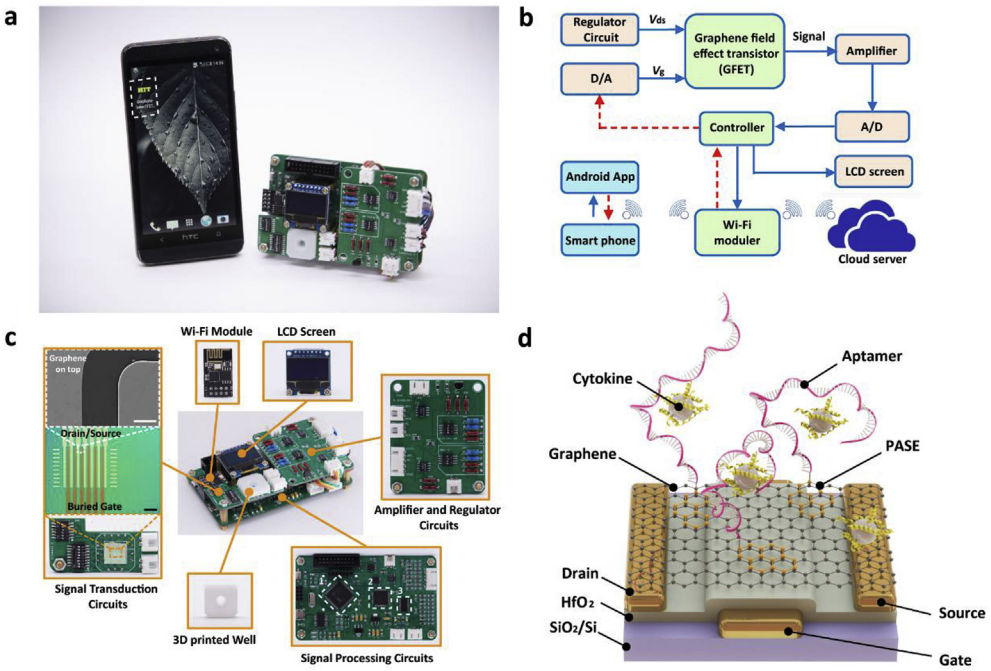

Fig. 1. Images and schematic illustrations of the aptameric GFET nanosensing system for cytokines detection. (a) Photograph of a fully integrated portable graphene-based nanosensing system with an Android smart phone. The white dashed box: Customized App for wireless display of the cytokine level information. (b) System-level block diagram of the nanosensing system showing the power supply (V_{ds} and V_g), signal (I_{ds}) transduction, processing, display and wireless transmission paths from portable nanosensing system to the smart phone and cloud server, respectively. (c) Photographs of a GFET nanosensing system. The white dashed boxes in Signal Processing Circuits block indicate the locations of the integrated circuit principal components: 1. ADS 1274 for data acquisition, 2. STM 32F4 for communication, 3. DAC 8830 for gate voltage supply. The orange dashed boxes in Signal Transduction Circuits block: Micrograph of a fabricated GFET with a buried-gate geometry. The graphene conducting channel connects the drain and source electrodes with a golden gate electrode buried in a 30 nm HfO_2 dielectric layer underneath. Scale bar: 100 μm. Inset dashed white box: SEM image of part of the graphene channel. Scale bar: 5 μm. (d) Schematic of the aptameric GFET with the buried-gate geometry for cytokine detection. (For interpretation of the references to colour in this figure legend, the reader is referred to the Web version of this article.)

processing circuits was listed in the Supporting Information.

2.2. Nanosensor fabrication

The fabrication protocol was illustrated in Fig. S2, the 285 nm SiO_2/Si employed as the substrate of the nanosensor was cleaned successively with acetone, isopropanol (IPA) and deionized water, finally dried by N_2 and treated by oxygen plasma. The buried gate electrode was fabricated *via* a bilayer lift-off photolithography process. Two layers of resist (sacrificial layer LOR 3A and photoresist AZ 1512) were sequentially spin-coated on the substrate using spin coater. The planar gate electrode consisting of a Cr/Au structure (2 nm/43 nm) were defined on the SiO_2/Si substrate using standard photolithography and metal deposition techniques. A 30 nm HfO_2 thick nanolayer that employed as the high-κ dielectric layer was subsequently coated on the top of gate electrode using Atomic Layer Deposition System. Then, the photolithography and metal deposition were repeated on the HfO_2 surface to define the drain/source electrodes consisting of a Cr/Au (2 nm/43 nm) structure.

Subsequently, the nanosensor was exposed to oxygen plasma to remove the remaining residue on the surface. The synthesized CVD graphene was then transferred onto the substrate through the well-known wet floating-transfer technique. Details can be found in our previous study (Hao et al., 2018).

2.3. Biochemical functionalization

To immobilize the aptamer onto the graphene channel, the nanosensor was first immersed in 5 mM PASE solution for 2 h at room temperature and sequentially rinsed with pure DMF to remove any free PASE. The PASE works as the linker containing a pyrenyl group, can irreversibly interact with graphene through π-π stacking. The nanosensor was then rinsed with 1X PBS followed by incubation with 100 nM aptamer solution overnight at room temperature. After rinsing with 1X PBS, 100 mM ethanolamine was added onto the graphene channel for 1 h to deactivate and block the excess reactive groups remaining on the graphene surface (Fig. S3). Later, the nanosensor chip was fixed onto the PCB board by Kapton tape with electrodes connected to the on-board bonding pads using silver epoxy glue and copper wires. Finally, a 3D printed open well was mounted on the nanosensor for liquid handling.

2.4. Preparation of IL-6 samples

To prepare IL-6 testing solutions dissolved with gargle, 10 μL of commercial gargle was added to 1 mL flask with 990 μL 1X PBS. Then, the mixture was shaken on a Vortex for 2 min to make it homogeneous and finally stored at 4 °C before IL-6 solution configurations.

Stimulated human saliva samples were collected from healthy volunteers (1#: female, 24 years, 2#: male, 28 years, 3#: male, 24 years) according to a recognized standard sampling procedure (Barhoumi et al., 2018; Bellagambi et al., 2017). Briefly, the saliva sampling was performed using the sterile synthetic swab purchased from Salivette (Sarstedt, Germany) as sampling device. The volunteer was asked to move the swab 2 min in the oral cavity at a self-selected pace. Saliva was then recovered by centrifugation of the swabs at 5000 rpm for 5 min at room temperature (20 °C). Subsequently, a constant volume (10 μL) of the centrifuged suspension was decanted to a volumetric flask with 9990 μL of 1X PBS to reach a final volume of 10 mL. Likewise, the mixture was shaken on a Vortex for 2 min to make it homogeneous and then stored at 4 °C before IL-6 solution configurations.

Finally, the IL-6 lyophilized powder was dissolved to a given concentration with 1X PBS, abovementioned gargle solution and saliva solution, respectively.

2.5. Liquid handling

During the test, a volume of 30 μL IL-6 (GH or EGF) at a given concentration is added to, and removed from the 3D printed open well using a pipetted (Fig. S4). No surface rinsing operation is employed during the solution replacement process.

2.6. Nanosensing system circuits design

The system consisting of three pieces of PCB boards including signal transduction circuits, signal processing circuits, amplifier circuits and regulator circuits (Fig. 1c), is powered by rechargeable nickel-metal hydride batteries (4.8–5.2 V, 1800 mAh). The negative power supply (−5 V) and +3.3 V for controller, chips and Wi-Fi module are all converted from the power supply through the on board customized circuits.

The circuit diagrams of the signal amplifying and V_g/V_{ds} power supply, which are the principal parts in the system are shown in Fig. 1c. The GFET nanosensor is fixed on the signal transduction board. Because the binding induced change in I_{ds} is weak (~0.01 or 0.1 μA), the commercial data collectors are not amenable to acquire accurate data for the subsequent analysis. Hence, we use an amplifier circuit to convert the original signal into a voltage signal (~1 or 10 mV). Then the amplified signal is collected by the analogue-to-digital converter ADS 1274 and processed by the build-in controller STM32F4 that shown in signal processing circuits board (Fig. 1c). Finally, the information can be either displayed on the LCD screen or transmitted to a smart phone or cloud server through a Wi-Fi module (Figs. S5a and b). As a result, we can monitor the IL-6 concentration information and set up sensor parameters such as V_g, through an Android App on the smart phone.

Also, the data can be collected and plotted on a computer with the help of a customized program through USB connection (Fig. S5c). The chips employed in the nanosensing system were listed and described in Table S1.

3. Results and discussion

3.1. Nanosensing system working principle

A 30 nm thick HfO_2 insulator layer under the graphene channel serves as the gate dielectric. A drain-source bias voltage V_{ds}, powered by the regulator circuit, generates a current I_{ds} through the graphene conducting channel. An external gate voltage V_g, which is offered by the output of a converter (DAC 8830, Texas Instruments), was fixed at an optimal value, where the graphene transconductance, as well as the GFET sensitivity, can reach its maximum.

As schematic diagram shown in Fig. 1b, an on-site signal processing circuit is employed to enable the on-line IL-6 detection. The original signal of the change in I_{ds}, which is used to determine the IL-6 level, is collected, conditioned, and processed with the aid of the on-board analyzer (ADS 1274, Texas Instruments) and controller (STM 32F4, STMicroelectronics). Due to the computational and serial communication capabilities of the controller, the signal can be continuously transduced to the corresponding IL-6 concentration on the basis of a default calibration equation. The IL-6 concentration information is simultaneously displayed on the embedded LCD screen or wireless transmitted to the smart phone through the Wi-Fi module and plotted as a function of time with the help of a customized Android App (Fig. S5). Also, thanks to the integrated Wi-Fi wireless transceiver, the relevant information can be uploaded to cloud servers, thereby enabling remote monitoring of the health condition of patients for doctors. Details of circuits design are described in Experimental section and Supporting Information Figs. S5–7.

3.2. Characterization of biochemical functionalization

To verify the successful biochemical functionalization, the graphene surface was characterized after each functionalization step. Details in the surface biochemical functionalization can be found in Supporting Information. The G-band splitting (1619 cm^{-1}) observed in the Raman spectra suggests the coupling of graphene and the pyrene groups on PASE (Fig. 2a) (Dong et al., 2009). The thickness of the graphene channel was measured by the atomic force microscopy (AFM) after treatment of aptamer and is found to have increased from 0.3 to 2.3 nm (Fig. 2b), which is in good agreement with the reported values of aptamer thickness on graphene (Wang et al., 2015). Further, the corresponding I_{ds} before and after PASE and aptamer functionalization step, was measured with V_{ds} increasing from 0 to 10 mV at a fixed V_g of 0 V. It is obvious that the slope of the linear fit decreases monotonically from 5.48×10^{-3} to 4.89×10^{-3} and 4.31×10^{-3} after PASE and aptamer functionalization, respectively (Fig. 2c). Energy dispersive spectroscopy (EDS) shows that the graphene surface is coated with nitrogen and phosphorus, which are the constituent element of deoxynucleotides (Fig. 2d and e). Considering these experimental results, it can be concluded that aptamer is successfully functionalized on the graphene channel (An et al., 2013; Kwon et al., 2012).

3.3. Detection of IL-6 in artificial samples

The cytokine detecting capability of the GFET nanosensing system was studied with the sensing area exposure to IL-6 in artificial sample solutions. Here, V_a is defined as the amplified signal of the drain-source current I_{ds} with $V_a = I_{ds} \times R_a$, where R_a is the zoom resistance. $\Delta V_a = V_a\text{-}V_0$, where V_0 is the value of V_a measured in fresh buffer at the beginning. The maximum value of ΔV_a, is denoted as$\Delta V_{a,max}$. Time-resolved measurements of IL-6 were performed with fixed V_{ds} = 13 mV and V_g = 17 mV in 1X PBS and commercial gargle solution, respectively. The commercial gargle, whose main components are NaCl solution, flaxseed gum and carboxymethyl chitosan, is a kind of artificial saliva and typically used for releasing the discomfort of individuals who suffer from xerostomia. To examine the IL-6 detection capability in different oral extracts, the commercial gargle was used as one of the testing solutions. As shown in Fig. 3a, the ratio ofΔV_a and $\Delta V_{a,max}$ increases stepwise and sharply from 0 to 0.84 with increasing IL-6 concentrations from fresh gargle solution to 2.5 nM and reaches 0.98 at 20 nM. The binding is likely to become saturated with IL-6 concentration above 20 nM as the $\Delta V_a/\Delta V_{a,max}$ value is almost invariable even after 100 nM IL-6 application. Also, it can be easily found that the binding of aptamer and IL-6 can reach equilibrium within 6 min at different concentrations. The same experiment was carried out with 1X PBS (Fig. S8), in which similar phenomenon was observed. The equilibrium value of$\Delta V_a/\Delta V_{a,max}$ with error bars obtained using three different devices is plotted as a function of IL-6 concentrations in Fig. 3b. The relationship between them can be described by a Hill-Langmuir equation (Ohno et al., 2010).

$$\Delta V_a = \Delta V_{a,\max} \frac{C_i}{C_i + K_D} \quad (1)$$

where C_i is the concentration of IL-6 and K_D is the binding equilibrium constant. The lower K_D indicates the stronger binding tendency between aptamer and IL-6. According to the almost overlapped fitted curves for 1X PBS and gargle solution, K_D are estimated to be 0.207 and 0.167 nM respectively, suggesting consistent IL-6 sensing performance are achieved by the nanosensing system in different artificial solutions.

3.4. Time-resolved control experiments

To verify the inertness of graphene to IL-6, time-resolved measurements were carried out by exposing the graphene channel to IL-6 without prior biochemical treatment (Ohno et al., 2009). As shown in the top graph of Fig. 4a, $\Delta V_a/V_0$ is almost kept constant at 1.0 with sequential application of IL-6 in 1X PBS at 20, 100, 400 and 1000 nM. Considering these results, IL-6 is more likely not to adsorb to the untreated graphene surface during testing period time (~15 min) or the adsorption does not introduce significant variation in the graphene conductivity at abovementioned concentrations. Therefore, graphene is appropriate for IL-6 detection.

To examine the specificity of the nanosensor to IL-6, real-time

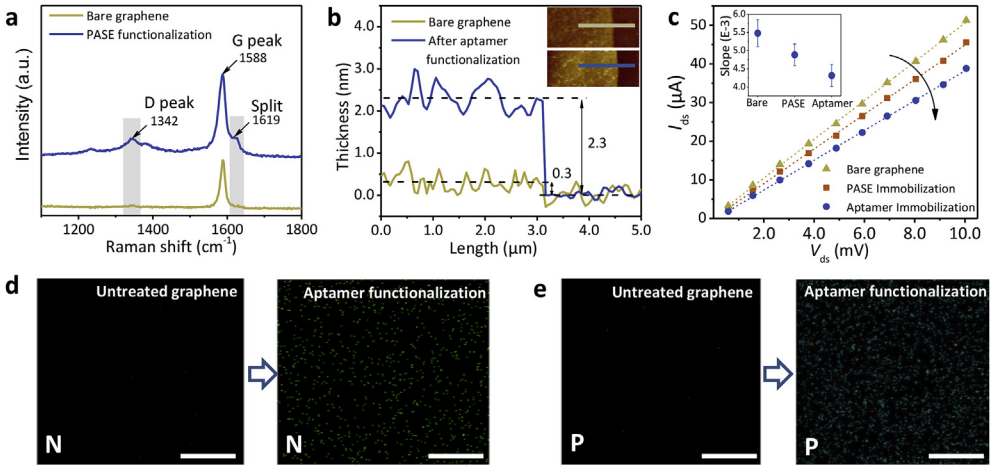

Fig. 2. Characterization of biochemical functionalization. (a) Raman spectra of graphene before and after exposure to the PASE solution. Signature peaks (1342 and 1619 cm^{-1}) of the noncovalent π−π interaction between PASE and graphene are observed after immersion in the PASE solution. (b) AFM images showing the scan lines plotted in the main figure. Scan lines are 4 μm. Z-scale 10 nm. The thickness of graphene channel is found to increase from 0.3 to 2.3 nm after aptamer immobilization. (c) Current-Voltage curves of the GFET nanosensor before and after PASE and aptamer functionalization. Inset: Slope is found to decrease stepwise after each functionalization step. Energy dispersive spectroscopy (EDS) shows that the deoxynucleotides constituent element nitrogen (d) and phosphorus (e) are widely coated on the graphene surface after exposure to the aptamer solution, indicating the successful aptamer functionalization. Scale bar in (d) and (e): 10 μm.

monitoring measurements were performed with the graphene channel exposure to non-target molecules in 1X PBS after biofunctionalization of IL-6 specific aptamers. Sharing similar physical properties with IL-6, EGF and GH were chosen as the negative control molecules. As displayed in the middle and bottom graphs of Fig. 4a, the value of $\Delta V_a/V_0$ for either GH or EGF curves is not varied significantly with increasing concentrations up to 100 nM. The maximum value of the variation in $\Delta V_a/V_0$ for EGF and GH control experiments are 1.5% and 2.1% respectively, which are almost 7 times smaller than the 13.8% obtained in IL-6 at same concentration (100 nM) (Fig. 4b). Consequently, high selectivity of the nanosensor to IL-6 by using the aptamer with a specific sequence to IL-6 is achieved.

3.5. Detection of IL-6 in human saliva

In view of the potential daily in-home use of this nanosensing system for monitoring cytokines, the validity of the nanosensing system for real-time detection of IL-6 in real human saliva solution was investigated. The human saliva solution was prepared as described in the experimental section. Different from artificial solutions, there are numerous non-target molecules and contaminations in saliva that might potentially and nonspecifically interact with graphene or aptamer. However, the results of graphene surface characterization using AFM suggest that the thickness of the graphene channel is kept constant at 2.3 nm all through before and after the exposure of aptamer functionalized graphene surface to saliva solution over 1 h (Fig. 5a and b). As a result, the potential effect from the unwanted interaction between graphene or aptamer and the non-target molecules was negligible.

Subsequently, IL-6 detection in saliva solution was carried out in real-time with increasing concentrations from fresh to 100 nM. Consistent detection results as observed in artificial solutions were obtained. The value of$\Delta V_a/\Delta V_{a,max}$ rises monotonically to 0.99 with an increase in the IL-6 concentration of under 20 nM and then remained approximately constant at 1.0 with addition of IL-6 at concentrations above 20 nM (Fig. 5c). Likewise, the equilibrium value at corresponding IL-6 concentration is plotted and fitted using Equation (1) in Fig. 4d with an estimated K_D of 0.113 nM (Fig. 5d), which is in agreement with abovementioned values in artificial solutions. Further, it can be obviously found that the $\Delta V_a/\Delta V_{a,max}$ value versus logarithm IL-6 concentration curves show a certain linear relationship within physiologically relevant levels and can be described with the following equation.

$$\frac{\Delta V_a}{\Delta V_{a,\max}} = k \times \log C_i + b \quad (2)$$

where k is the slope of the linear fit curve and b is the intercept on y axis. In accordance with the 3σ/slope calculation rule, the limit of detection (LOD) for our nanosensing system are estimated to be 10.5, 11.8 and 12.2 pM in 1X PBS, artificial gargle solution and human saliva solution, respectively (Fig. 5e). These values of LOD are all within the physiological IL-6 level in human bodily fluids, thereby potentially enabling the practical application of the nanosensing system for IL-6 detection in human saliva in daily.

To exclude the potential effect from the time drift of the GFET nanosensor on the sensing performance, the time-resolved response of the nanosensor was investigated with exposure to various fresh buffers. Considering the evaporation issue, the buffer solutions in the open well was duly replenished during the 1 h testing period. As shown in Fig. 5f, the maximum value of the variation in$\Delta V_a/V_0$ are 0.35%, 0.38% and 0.40% for 1X PBS, gargle solution and human saliva solution, respectively. It can be conclude that the effect induced by the time drift of the GFET nanosensor on the response signal of IL-6 detection is negligible.

Furthermore, to study the possible effect induced by the non-

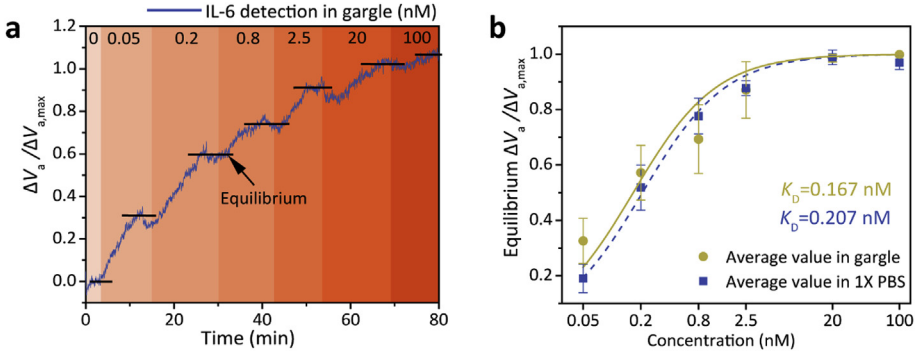

Fig. 3. Detection of IL-6 in artificial samples. (a) Time-resolved measurements of changes in the IL-6 concentration using gargle solution. The responses are demonstrated by $\Delta V_a/\Delta V_{a,max}$. (b) Changes in the average value of equilibrium $\Delta V_a/\Delta V_{a,max}$ as a function of IL-6 concentrations (The average value and error bar were obtained from three devices). The dashed lines are a least-squares fit to the Hill−Langmuir equation, yielding equilibrium dissociation constant (K_D) of 0.167 and 0.207 nM in commercial gargle solution (red) and 1X PBS (green), respectively. (For interpretation of the references to colour in this figure legend, the reader is referred to the Web version of this article.)

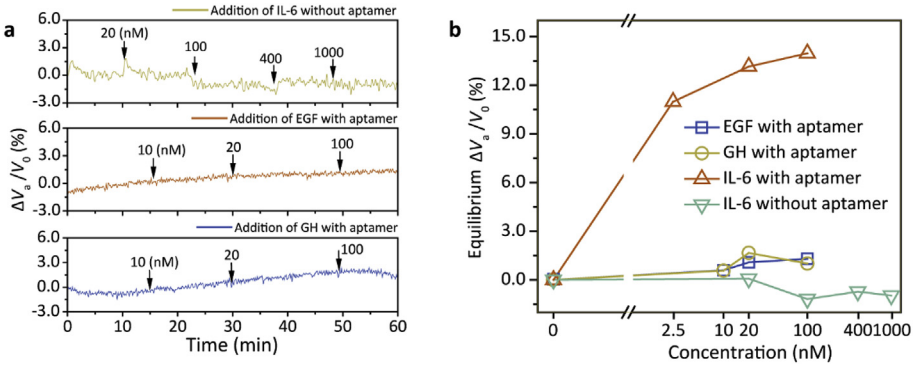

Fig. 4. Selective response of the GFET nanosensor to IL-6 in 1X PBS. (a) Time-resolved control experiments with untreated graphene channel exposure to IL-6 at various concentrations (20, 100, 400 and 1000 nM) and aptamer functionalized graphene channel exposure to solutions of EGF and GH at given concentrations (10, 20 and 100 nM). (b) Equilibrium value of $\Delta V_a/V_0$ measured with and without aptamers in different solutions (EGF/GH/IL-6) is plotted as a function of given concentrations, respectively.

uniformity of the different saliva solution from individuals on the IL-6 detection capability, IL-6 monitoring experiments were performed with prepared saliva solutions from three nominally healthy volunteers (Fig. 6a). As shown in Fig. 6b, at each given IL-6 concentration, the value of $\Delta V_a/\Delta V_{a,max}$ does not vary significantly, with fluctuation less than 7.47% and a maximum coefficient of variation (CV) of 0.12077, suggesting that the validity for practical IL-6 detection in different real human saliva solutions is achieved by the developed nanosensing system. However, components of real saliva are complex while individual-to-individual non-uniformities would make it more difficult to eliminate uncertain interferences effect on the sensing performance especially in the low IL-6 concentration range (< 200 pM). Works still need to be done to minimize the effect from the non-uniformities of different real samples.

4. Conclusions

In this work, a graphene-based fully integrated portable nanosensing system for highly sensitive and specific on-line detection of salivary cytokine biomarkers such as IL-6, was presented. The system employs an aptameric GFET nanosensor with a buried-gate geometry and on-line signal processing circuits to realize the transduction and processing of signals that in relation to IL-6 concentrations. The signal can be not only displayed on the embedded LCD screen but also wirelessly transmitted to a smart-phone or cloud sever through the Wi-Fi connection for visualizing the trend of the IL-6 concentration change. First, the specificity of the nanosensor to IL-6 was examined, real-time monitoring experimental results indicate that high selectivity of the nanosensor to IL-6 over other related negative control molecules such as GH and EGF, is achieved. Second, the portable sensing device can respond to IL-6 concentration changes within few minutes in 1X PBS, gargle solution and human saliva solution with detection limits down to 10.5, 11.8 and 12.2 pM, respectively, which are within the physiological level of IL-6 in the human body. Finally, the possible effect induced by the individual-to-individual nonuniformity on the IL-6 detection capability in three different volunteer saliva solutions was studied. The measured response signal does not vary significantly with fluctuation less than 7.47%. The fluctuation might be caused by the unknown interferences resulted from the nonuniformity of different real saliva samples. Our future work would address such issue and enhance the sensing stability by protecting graphene surface from interactions with background non-target molecules in real saliva. Nevertheless, our portable graphene-based nanosensing system holds great potential to be used for clinical diagnosis of diseases at their early stage.

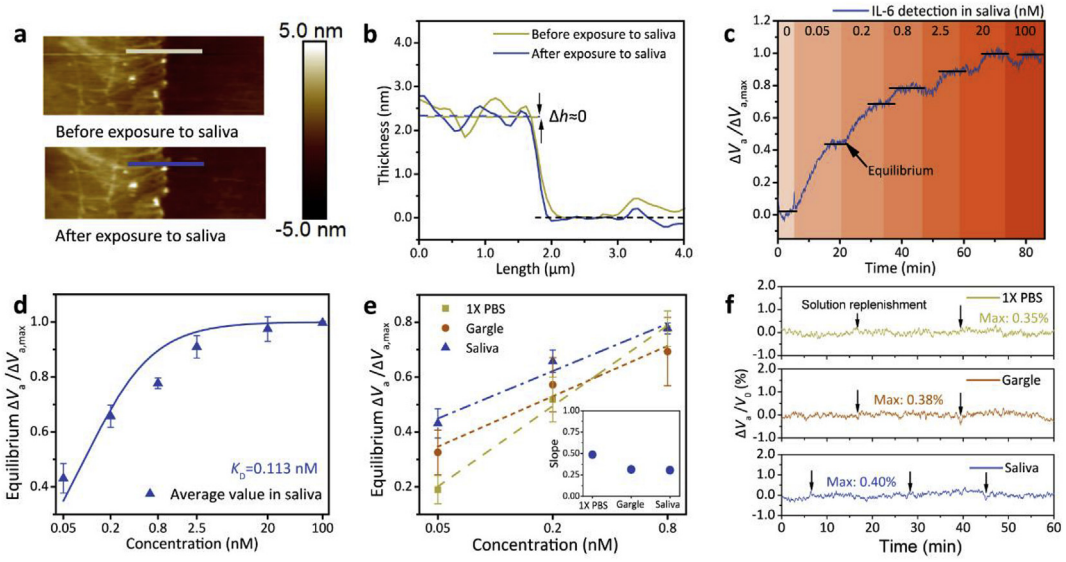

Fig. 5. Detection of IL-6 in human saliva solution. (a) AFM images of the graphene channel before and after exposure to human saliva solution for 30 min. Scan lines are 4 μm. (b) The thickness of the graphene channel before and after saliva solution addition process is approximately constant. (c) Time-resolved measurements of variations in the concentration of IL-6 dissolved in human saliva solution. (d) Equilibrium $\Delta V_a/\Delta V_{a,max}$ values as a function of IL-6 concentrations with a least-squares fit dashed curve (The average value and error bar were obtained from three devices). K_D is estimated to be 0.113 nM. (e) Linear fit of $\Delta V_a/\Delta V_{a,max}$ with logarithm increasing IL-6 concentrations from 50 to 800 pM in the given solution (1X PBS/gargle solution/saliva solution). Inset: Slope value of the linear fitted curves of given solutions. (f) Time drift in the response of the nanosensing system after exposure to various buffers of 1X PBS, gargle solution and saliva solution in 1 h. The maximum variation values of 0.35% (1X PBS), 0.38% (gargle solution) and 0.40% (saliva solution) in given solutions are negligible.

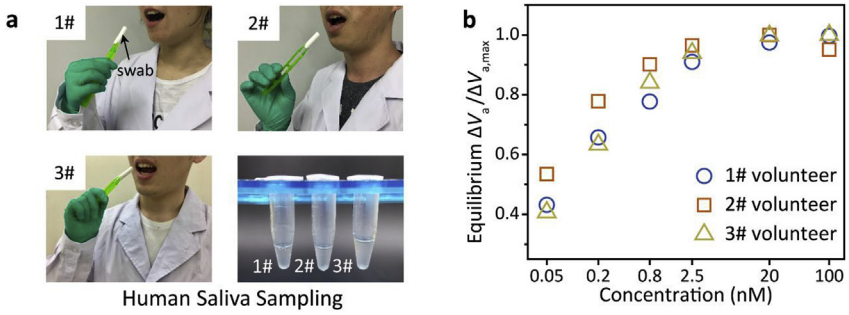

Fig. 6. Detection of IL-6 in human saliva solutions from different individuals. (a) Saliva sample collection. The 1# (top left), 2# (top right), and 3# (bottom left) volunteer put the swab into the oral cavity separately. Bottom right displays the saliva suspension samples after centrifugation. (b) Changes in $\Delta V_a/\Delta V_{a,max}$ that obtained in three individual saliva solutions as a function of IL-6 concentrations ranging from 50 pM to 100 nM.

CRediT authorship contribution statement

Zhuang Hao: Conceptualization, Methodology, Data curation, Formal analysis, Writing - original draft, Visualization, Writing - review & editing. **Yunlu Pan:** Methodology, Validation, Writing - review & editing, Funding acquisition, Project administration. **Wenwen Shao:** Software. **Qiao Lin:** Writing - review & editing. **Xuezeng Zhao:** Funding acquisition, Project administration.

Acknowledgements

This work was supported by fundings from the National Natural Science Foundation of China (Grant Nos. 51505108 and 51475118). The author Zhuang Hao would like to gratefully thank Mr. Yang Luo, and Dr. Hui Xie from State Key Laboratory of Robotics and System at Harbin Institute of Technology and Dr. James Hone, and Dr. Yibo Zhu from Department of Mechanical Engineering at Columbia University for technical supports and insightful discussions.

Appendix A. Supplementary data

Supplementary data to this article can be found online at https://doi.org/10.1016/j.bios.2019.03.053.

References

Afsahi, S., Lerner, M.B., Goldstein, J.M., Lee, J., Tang, X., Bagarozzi, D.A., Pan, D., Locascio, L., Walker, A., Barron, F., Goldsmith, B.R., 2018. Novel graphene-based biosensor for early detection of Zika virus infection. Biosens. Bioelectron. 100, 85–88. https://doi.org/10.1016/j.bios.2017.08.051.

An, J.H., Park, S.J., Kwon, O.S., Bae, J., Jang, J., 2013. High-performance flexible graphene aptasensor for mercury detection in mussels. ACS Nano 7, 10563–10571. https://doi.org/10.1021/nn402702w.

Arakawa, T., Kuroki, Y., Nitta, H., Chouhan, P., Toma, K., Sawada, S. ichi, Takeuchi, S., Sekita, T., Akiyoshi, K., Minakuchi, S., Mitsubayashi, K., 2016. Mouthguard biosensor with telemetry system for monitoring of saliva glucose: a novel cavitas sensor. Biosens. Bioelectron. 84, 106–111. https://doi.org/10.1016/j.bios.2015.12.014.

Barhoumi, L., Baraket, A., Bellagambi, F.G., Karanasiou, G.S., Ali, M., Ben Fotiadis, D.I., Bausells, J., Zine, N., Sigaud, M., Errachid, A., 2018. A novel chronoamperometric immunosensor for rapid detection of TNF-α in human saliva. Sensor. Actuator. B Chem. 266, 477–484. https://doi.org/10.1016/j.snb.2018.03.135.

Bariya, M., Nyein, H.Y.Y., Javey, A., 2018. Wearable sweat sensors. Nat. Electron. 1, 160–171. https://doi.org/10.1038/s41928-018-0043-y.

Bellagambi, F.G., Baraket, A., Longo, A., Vatteroni, M., Zine, N., Bausells, J., Fuoco, R., Di Francesco, F., Salvo, P., Karanasiou, G.S., Fotiadis, D.I., Menciassi, A., Errachid, A., 2017. Electrochemical biosensor platform for TNF-α cytokines detection in both artificial and human saliva: heart failure. Sensor. Actuator. B Chem. 251, 1026–1033. https://doi.org/10.1016/j.snb.2017.05.169.

Blay, J.Y., Negrier, S., Combaret, V., Attali, S., Goillot, E., Merrouche, Y., Mercatello, A., Ravault, A., Tourani, J.M., Moskovtchenko, J.F., et al., 1992. Serum level of interleukin 6 as a prognosis factor in metastatic renal cell carcinoma. Cancer Res. 52, 3317–3322.

Cai, B., Wang, S., Huang, L., Ning, Y., Zhang, Z., Zhang, G.J., 2014. Ultrasensitive label-free detection of PNA-DNA hybridization by reduced graphene oxide field-effect transistor biosensor. ACS Nano 8, 2632–2638. https://doi.org/10.1021/nn4063424.

Campos, A.M., Raymundo-Pereira, P.A., Mendonça, C.D., Calegaro, M.L., Machado, S.A.S., Oliveira, O.N., 2018. Size control of carbon spherical shells for sensitive detection of paracetamol in sweat, saliva, and urine. ACS Appl. Nano Mater. 1, 654–661. https://doi.org/10.1021/acsanm.7b00139.

Chekin, F., Vasilescu, A., Jijie, R., Singh, S.K., Kurungot, S., Iancu, M., Badea, G., Boukherroub, R., Szunerits, S., 2018. Sensitive electrochemical detection of cardiac troponin I in serum and saliva by nitrogen-doped porous reduced graphene oxide electrode. Sensor. Actuator. B Chem. 262, 180–187. https://doi.org/10.1016/j.snb.2018.01.215.

Chen, J.H., Jang, C., Adam, S., Fuhrer, M.S., Williams, E.D., Ishigami, M., 2008. Charged-impurity scattering in graphene. Nat. Phys. 4, 377–381. https://doi.org/10.1038/nphys935.

Dong, X., Fu, D., Fang, W., Shi, Y., Chen, P., Li, L.J., 2009. Doping single-layer graphene with aromatic molecules. Small 5, 1422–1426. https://doi.org/10.1002/smll.200801711.

Emaminejad, S., Gao, W., Wu, E., Davies, Z.A., Yin Yin Nyein, H., Challa, S., Ryan, S.P., Fahad, H.M., Chen, K., Shahpar, Z., Talebi, S., Milla, C., Javey, A., Davis, R.W., 2017. Autonomous sweat extraction and analysis applied to cystic fibrosis and glucose monitoring using a fully integrated wearable platform. Proc. Natl. Acad. Sci. Unit. States Am. 114, 4625–4630. https://doi.org/10.1073/pnas.1701740114.

Fan, G., Ren, X., Zhu, C., Zhang, J., Zhu, J., 2014. Biosensors and Bioelectronics A new signal ampli fi cation strategy of photoelectrochemical immunoassay for highly sensitive interleukin-6 detection based on TiO 2/CdS/CdSe dual co-sensitized structure. Biosens. Bioelectron. 59, 45–53. https://doi.org/10.1016/j.bios.2014.03.011.

Gao, W., Emaminejad, S., Nyein, H.Y.Y., Challa, S., Chen, K., Peck, A., Fahad, H.M., Ota, H., Shiraki, H., Kiriya, D., Lien, D.H., Brooks, G.A., Davis, R.W., Javey, A., 2016. Fully integrated wearable sensor arrays for multiplexed in situ perspiration analysis. Nature 529, 509–514. https://doi.org/10.1038/nature16521.

Gasche, J.A., Hoffmann, J., Boland, C.R., Goel, A., 2011. Interleukin-6 promotes tumorigenesis by altering DNA methylation in oral cancer cells. Int. J. Cancer 129, 1053–1063. https://doi.org/10.1002/ijc.25764.

Hao, Z., Wang, Z., Li, Y., Zhu, Y., Wang, X., De Moraes, C.G., Pan, Y., Zhao, X., Lin, Q., 2018. Measurement of cytokine biomarkers using an aptamer-based affinity graphene nanosensor on a flexible substrate toward wearable applications. Nanoscale 21681–21688. https://doi.org/10.1039/C8NR04315A.

Hao, Z., Zhu, Y., Wang, X., Rotti, P.G., Dimarco, C., Tyler, S.R., Zhao, X., Engelhardt, J.F., Hone, J., Lin, Q., 2017. Real-time monitoring of insulin using a graphene field-effect transistor aptameric nanosensor. ACS Appl. Mater. Interfaces 9, 27504–27511. https://doi.org/10.1021/acsami.7b07684.

Khosravi, F., Loeian, S.M., Panchapakesan, B., 2017. Ultrasensitive label-free sensing of IL-6 based on PASE functionalized carbon nanotube micro-arrays with RNA-aptamers as molecular recognition elements. Biosensors 7. https://doi.org/10.3390/bios7020017.

Kim, J., Imani, S., de Araujo, W.R., Warchall, J., Valdés-Ramírez, G., Paixão, T.R.L.C., Mercier, P.P., Wang, J., 2015. Wearable salivary uric acid mouthguard biosensor with integrated wireless electronics. Biosens. Bioelectron. 74, 1061–1068. https://doi.org/10.1016/j.bios.2015.07.039.

Kim, J., Kim, M., Lee, M.S., Kim, K., Ji, S., Kim, Y.T., Park, J., Na, K., Bae, K.H., Kim, H.K., Bien, F., Lee, C.Y., Park, J.U., 2017. Wearable smart sensor systems integrated on soft contact lenses for wireless ocular diagnostics. Nat. Commun. 8, 1–8. https://doi.org/10.1038/ncomms14997.

Kim, J., Valdés-Ramírez, G., Bandodkar, A.J., Jia, W., Martinez, A.G., Ramírez, J., Mercier, P., Wang, J., 2014. Non-invasive mouthguard biosensor for continuous salivary monitoring of metabolites. Analyst 139, 1632–1636. https://doi.org/10.1039/C3AN02359A.

Kwon, O.S., Park, S.J., Hong, J.Y., Han, A.R., Lee, J.S., Lee, J.S., Oh, J.H., Jang, J., 2012. Flexible FET-Type VEGF aptasensor based on nitrogen-doped graphene converted from conducting polymer. ACS Nano 6, 1486–1493. https://doi.org/10.1021/nn204395n.

Li, Y., Wang, C., Zhu, Y., Zhou, X., Xiang, Y., He, M., Zeng, S., 2017. Fully integrated graphene electronic biosensor for label-free detection of lead (II) ion based on G-quadruplex structure-switching. Biosens. Bioelectron. 89, 758–763. https://doi.org/10.1016/j.bios.2016.10.061.

Liao, C., Mak, C., Zhang, M., Chan, H.L.W., Yan, F., 2015. Flexible organic electrochemical transistors for highly selective enzyme biosensors and used for saliva testing. Adv. Mater. 27, 676–681. https://doi.org/10.1002/adma.201404378.

Mannoor, M.S., Tao, H., Clayton, J.D., Sengupta, A., Kaplan, D.L., Naik, R.R., Verma, N., Omenetto, F.G., McAlpine, M.C., 2012. Graphene-based wireless bacteria detection on tooth enamel. Nat. Commun. 3, 763–768. https://doi.org/10.1038/ncomms1767.

Ohno, Y., Maehashi, K., Matsumoto, K., 2010. Label-free biosensors based on aptamer-modified graphene field-effect transistors. J. Am. Chem. Soc. 132, 18012–18013. https://doi.org/10.1021/ja108127r.

Ohno, Y., Maehashi, K., Yamashiro, Y., Matsumoto, K., 2009. Electrolyte-gated graphene field-effect transistors for detecting pH and protein adsorption. Nano Lett. 9, 3318–3322. https://doi.org/10.1021/nl901596m.

Park, J., Kim, J., Kim, S.Y., Cheong, W.H., Jang, J., Park, Y.G., Na, K., Kim, Y.T., Heo, J.H., Lee, C.Y., Lee, J.H., Bien, F., Park, J.U., 2018. Soft, smart contact lenses with integrations of wireless circuits, glucose sensors, and displays. Sci. Adv. 4, 1–12. https://doi.org/10.1126/sciadv.aap9841.

Ping, J., Vishnubhotla, R., Vrudhula, A., Johnson, A.T.C., 2016. Scalable production of high-sensitivity, label-free DNA biosensors based on back-gated graphene field effect transistors. ACS Nano 10, 8700–8704. https://doi.org/10.1021/acsnano.6b04110.

Pruna, R., Palacio, F., Baraket, A., Zine, N., Streklas, A., Bausells, J., Errachid, A., López, M., 2018. A low-cost and miniaturized potentiostat for sensing of biomolecular species such as TNF-α by electrochemical impedance spectroscopy. Biosens. Bioelectron. 100, 533–540. https://doi.org/10.1016/j.bios.2017.09.049.

Santana-Jiménez, L.A., Márquez-Lucero, A., Osuna, V., Estrada-Moreno, I., Dominguez, R.B., 2018. Naked-eye detection of glucose in saliva with bienzymatic paper-based sensor. Sensors 18, 1–12. https://doi.org/10.3390/s18041071.

Tseng, P., Napier, B., Garbarini, L., Kaplan, D.L., Omenetto, F.G., 2018. Functional, RF-trilayer sensors for tooth-mounted, wireless monitoring of the oral cavity and food consumption. Adv. Mater. 1703257, 1–7. https://doi.org/10.1002/adma.201703257.

Van Der Heyden, F.H.J., Stein, D., Dekker, C., 2005. Streaming currents in a single nanofluidic channel. Phys. Rev. Lett. 95. https://doi.org/10.1103/PhysRevLett.95.116104.

Wang, C., Kim, J., Zhu, Y., Yang, J., Lee, G.H., Lee, S., Yu, J., Pei, R., Liu, G., Nuckolls, C., Hone, J., Lin, Q., 2015. An aptameric graphene nanosensor for label-free detection of small-molecule biomarkers. Biosens. Bioelectron. 71, 222–229. https://doi.org/10.1016/j.bios.2015.04.025.

Wang, C., Li, Y., Zhu, Y., Zhou, X., Lin, Q., He, M., 2016. Correction to: high-κ solid-gate transistor configured graphene biosensor with fully integrated structure and enhanced sensitivity. 2016. Adv. Funct. Mater. 26 (42), 7668–7678. https://doi.org/10.1002/adfm.201602960. Adv. Funct. Mater. 26, 8575. https://doi.org/10.1002/adfm.201605733.

Wang, X., Zhu, Y., Olsen, T.R., Sun, N., Zhang, W., Pei, R., Lin, Q., 2018. A graphene aptasensor for biomarker detection in human serum. Electrochim. Acta 290, 356–363. https://doi.org/10.1016/j.electacta.2018.08.062.

Yang, Y., Gao, W., 2018. Wearable and flexible electronics for continuous molecular monitoring. Chem. Soc. Rev. 48, 1465–1491. https://doi.org/10.1039/C7CS00730B.

Yang, Y., Yang, X., Zou, X., Wu, S., Wan, D., Cao, A., Liao, L., Yuan, Q., Duan, X., 2017. Ultrafine graphene nanomesh with large on/off ratio for high-performance flexible biosensors. Adv. Funct. Mater. 27, 1–9. https://doi.org/10.1002/adfm.201604096.

Zhu, Y., Wang, C., Petrone, N., Yu, J., Nuckolls, C., Hone, J., Lin, Q., 2015. A solid dielectric gated graphene nanosensor in electrolyte solutions. Appl. Phys. Lett. 106. https://doi.org/10.1063/1.4916341.